J. Fluid Mech. (2017), *vol.* 829, R1, doi:10.1017/jfm.2017.590

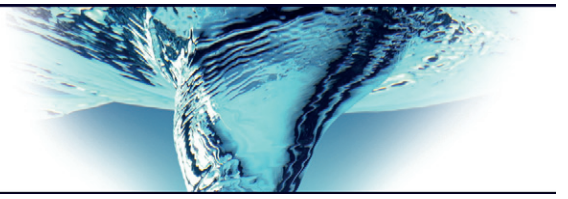

JFM RAPIDS
journals.cambridge.org/rapids

Forcing symmetry exchanges and flow reversals in turbulent wakes

Diogo Barros[1,†], Jacques Borée[1], Olivier Cadot[2], Andreas Spohn[1] and Bernd R. Noack[3,4]

[1]Institut Pprime UPR-3346, CNRS – Université de Poitiers – ENSMA, Poitiers 86360, France

[2]IMSIA, ENSTA–ParisTech/CNRS/CEA/EDF, Université Paris Saclay, Palaiseau 91762, France

[3]LIMSI – CNRS UPR 3251, Campus Universitaire d'Orsay, Orsay 91405, France

[4]Institut für Strömungsmechanik, TU Braunschweig, Braunschweig 38108, Germany

(Received 15 March 2017; revised 23 July 2017; accepted 17 August 2017;
first published online 14 September 2017)

Turbulent wakes past bluff bodies commonly present asymmetric flow states reminiscent of bifurcations in the laminar regime. Understanding the sensitivity of these states to flow forcing is crucial to the modelling and control of flow symmetry properties. In this study, the near wake of a rectangular bluff body in proximity to a wall is disturbed by the use of passive devices located between the model and the wall, upstream of the massive flow separation occurring at the blunt trailing edges. Due to the proximity to the boundary, the wake initially presents wall-normal asymmetry and a negative wall-normal pressure gradient along the base. The application of disturbances with variable size, however, sets flow symmetry along the wall-normal plane, leading to the intermittent spanwise wake reversals reported recently in the literature. A further increase in the size of perturbation suppresses wake switching, and wall-normal asymmetry is recovered, but with a positive wall-normal pressure gradient. The dynamical features of this bifurcation scenario can be retrieved using two coupled symmetry-breaking models for spanwise and wall-normal pressure gradients. This confirms the high sensitivity of the separated flow to external perturbations. More importantly, the results unify observations of the bluff-body wake topologies covered in previous investigations.

Key words: bifurcation, instability control, wakes

1. Introduction

Turbulent bluff-body wakes are characterized by complex interactions between flow instabilities associated with vortex shedding and the growth of shear layers.

† Present address: Department of Aerospace Engineering and Mechanics, University of Minnesota, Minneapolis, MN, USA. Email address for correspondence: dbarros@umn.edu

The structure of the recirculating flow in the near wake undergoes symmetry-breaking bifurcations in the laminar regime, leading to high levels of asymmetry of the separated flow (Fabre, Auguste & Magnaudet 2008; Grandemange, Cadot & Gohlke 2012; Marquet & Larsson 2015). In nominally axisymmetric configurations, the instantaneous near-wake flow is asymmetric but conditional averaging conducted by Grandemange, Gohlke & Cadot (2014) behind a sphere reveals the existence of planar symmetry with respect to a given azimuthal flow orientation θ_W. The probability distribution of θ_W in the long-time horizon is uniform, the wake is statistically symmetric but the instantaneous asymmetric flow randomly switches its azimuthal orientation with diffusive stochastic dynamics, as demonstrated similarly for blunt axisymmetric geometries with fixed flow separation (Rigas *et al.* 2014, 2015). This behaviour results from the infinite number of symmetry planes inherent to axisymmetry and helps in clarifying the insightful discussion in the seminal paper of Achenbach (1974) on the existence of a helical near-wake structure.

An equivalent situation occurs when the number of symmetry planes is finite, as in the case of bluff bodies with rectangular cross-sections. Depending on the height-to-width ratio of the cross-section, the wake presents top/bottom (for a base higher than it is wide) or lateral (for a base wider than it is high) asymmetries with preferred orientation highly sensitive to the proximity of the boundary, such as near walls commonly used to mimic the aerodynamics of ground vehicles (Grandemange, Gohlke & Cadot 2013*a*; Choi, Lee & Park 2014). It is worth mentioning the existence of an interfering region within the range of aspect ratio [0.77, 1.3] for which one asymmetry dominates the other due to the wall and body supports.

Recent experiments of Grandemange, Gohlke & Cadot (2013*b*) with an aspect ratio of 0.74, later confirmed by Volpe, Devinant & Kourta (2015), Brackston *et al.* (2016) and Perry, Pavia & Passmore (2016), show the existence of spanwise flow reversals (switching of states characterized by a bimodal distribution) of the asymmetric recirculating flow taking place in a plane parallel to the near wall. In these cases, the flow is nearly symmetric within the wall-normal symmetry plane crossing the base of the bluff body. Other numerical and experimental studies describe, instead, wall-normal wake asymmetries without reporting the bimodal flow behaviour in the wall-parallel plane for different values of aspect ratio ranging from 0.74 to 1.4 (Krajnovic & Davidson 2003; Wassen, Eichinger & Thiele 2010; Lahaye, Leroy & Kourta 2014; Barros *et al.* 2016*a*; McArthur *et al.* 2016).

It is interesting to inquire about the reasons behind the different flow states found in the literature, as an attempt to elucidate the nature of wake asymmetries thus conciliating contradictory investigations on this flow. We expect that further insight into the intriguing relation between symmetry planes and bimodal wake reversals can furnish new ideas to control the turbulent wake past bluff bodies with fixed symmetry planes. In the present experimental study, we artificially disturb the asymmetric flow past a rectangular bluff body in proximity to a wall using passive devices located between the model and the wall upstream of the trailing edges. By installing these devices to perturb the underbody flow, the symmetry properties of the recirculating region can be greatly altered without changing the flow conditions and geometry. In § 3, we analyse mean and dynamic changes of the wake using statistics of the pressure and velocity fields acquired from particle image velocimetry described in § 2. Then, we discuss the observed dynamic changes using an analogy with the symmetry-breaking dynamics contained in a stochastic Langevin model (§ 4), before providing our concluding remarks in § 5.

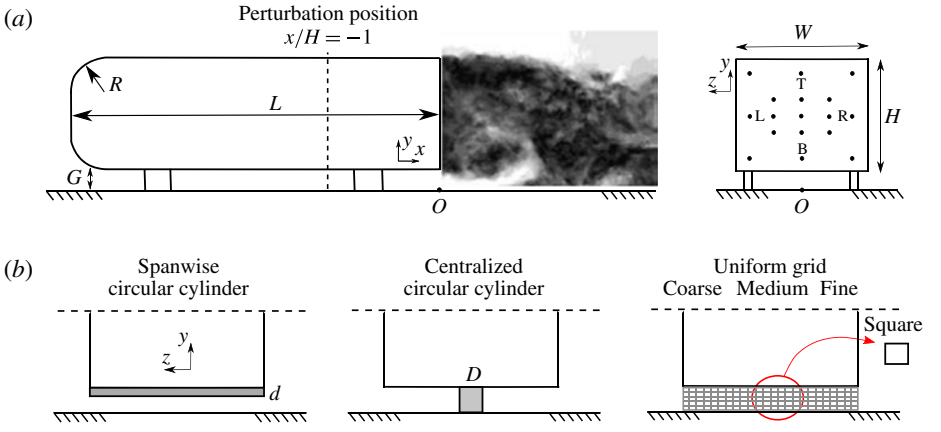

FIGURE 1. Sketch of the experimental set-up. (*a*) Bluff-body geometry and streamwise location ($x/H = -1$) where the perturbations are installed. The rear view indicates the pressure taps used on the rear surface of the model. (*b*) Types and arrangement of perturbations underneath the bluff body at streamwise location $x/H = -1$.

2. Methods

2.1. *Geometry and measurements*

The experiments are conducted inside a wind tunnel with test section dimensions of 2.4 m (width) and 2.6 m (height). The constant free-stream velocity is set to $U_o = 15\ \mathrm{m\ s^{-1}}$ with turbulence intensity of 0.5 %. The bluff-body geometry investigated here is shown in figure 1(*a*). It is placed over a flat plate installed in the working section. The reader is referred to Barros *et al.* (2016*b*) and references therein for details of the set-up. The model of height $H = 0.297$ m, width $W = 0.350$ m and length $L = 0.893$ m is fixed to the ground by four profiled supports of height $G = 0.05$ m. Its rectangular cross-section is similar to that in the seminal study of Ahmed, Ramn & Faltin (1984), but the aspect ratio of the model is higher ($H/W = 0.85$) in the present study. The resulting ground clearance is approximately five times higher than the oncoming boundary layer, which measures $\delta_{99} = 0.034H$ with displacement thickness $\delta^\star = 0.004H$ and shape factor $\overline{H} = 1.58$.

Based on the height of the model, the Reynolds number is $Re_H = U_o H/\nu = 3 \times 10^5$, where ν is the kinematic viscosity of the air at ambient temperature. We define the coordinate system using the streamwise (x), the transverse or wall-normal (y) and the spanwise (z) axes with the origin O arbitrarily located on the ground aligned to the base of the bluff body. Hereafter, all physical quantities presented without dimensions are normalized by U_o, H and the dynamic pressure $q_o = 0.5\rho {U_o}^2$, where ρ is the air density at ambient conditions.

The picture on the right of figure 1(*a*) illustrates the distribution of the pressure taps over the rear surface of the bluff body. They are connected to differential pressure sensors HCLA 02X5DB (SensorTechnics®) operating in a range of ±250 Pa with respect to the upstream static pressure p_o acquired with a Prandtl tube. The pressure coefficient for each measurement is defined as $C_p = (p - p_o)/q_o$. In order to detect asymmetric flow states in the wake, pressure measurements are conducted for a duration of 10 minutes with an acquisition frequency of 6.25 kHz, corresponding to more than 3×10^4 convective time units H/U_o or 6×10^3 vortex

shedding cycles (Barros *et al.* 2016*a*). For selected configurations, two additional tests confirmed the excellent repeatability of signal statistics. Following Grandemange *et al.* (2013*a*), we define the spanwise and wall-normal pressure differences respectively by $\delta_z = C_{pL} - C_{pR}$ and $\delta_y = C_{pT} - C_{pB}$, using pressure taps centred at the top (T), bottom (B), left (L) and right (R) as shown in the sketch. These quantities are used to determine the degree of flow asymmetry along the plane crossing the middle height of the model ($y/H = 0.67$) and the wall-normal symmetry plane of the configuration ($z = 0$), respectively.

Besides measurements of the pressure gradients along the rear surface of the model, planar particle image velocimetry (PIV) is used to analyse the structure of the near wake. (For the sake of simplicity, we use the term pressure gradient in opposition to pressure difference without compromising the physical significance of our subsequent analysis.) Two PIV fields of view allow us to obtain the velocity vectors in the symmetry ($z = 0$) and middle ($y/H = 0.67$) planes, both covering the entire recirculating flow domain. For that, we use two LaVision Imager pro X 4M cameras installed side by side to acquire images in both planes and to compute streamwise–transverse (u, v, symmetry plane) and streamwise–spanwise (u, w, middle plane) velocity components. The laser sheet is generated by an EverGreen Nd:YAG 532 nm (200 mJ) system and is pulsed using time delays of 120 µs synchronized to the cameras to perform acquisition of image pairs at 3.5 Hz. Velocity vectors are computed using Davis 8.2 with an interrogation window of 32×32 pixels and overlap of 50 %. The resulting spatial resolution is approximately 1 % of the model's height, and ensembles of 2000 independent velocity fields are used to obtain first- and second-order statistics of the flow.

2.2. *Passive disturbances*

Passive devices are installed upstream of the rear surface of the model at a fixed streamwise position $x/H = -1$. They are located between the ground and the lower surface of the bluff body, as schematized in figure 1(*b*). This location is not varied during the present experimental campaign. However, the robustness of the bifurcation scenario described in what follows was tested during preliminary measurements using perturbations installed closer to the trailing edge on a different bluff-body front geometry with a square back section. The use of these devices enables us to create disturbances that impact the developing shear flow in the proximity of the wall, thus triggering changes of entrainment rates in the wake. Such a modification of the underflow properties and mixing along the shear layer is capable of reversing the recirculating motion and the symmetry properties of the near wake (Barros *et al.* 2016*b*).

We consider three types of disturbances at different scales. A spanwise perturbation of the boundary layer is achieved by installing a circular cylinder with multiple diameters $d = \{0.020, 0.027, 0.054\}$ spanning over the whole width W of the model. Local perturbations of the underflow are produced by a vertical cylinder with variable diameter $D = \{0.027, 0.067, 0.084, 0.10, 0.17, 0.20, 0.24\}$, which is fixed in the symmetry plane of the model and extends over the whole height G of the underbody flow. Finally, coarse, medium and fine grids with mesh sizes of $\{6, 4, 2\}$ mm and grid wires of $\{1, 1, 0.5\}$ mm produce homogeneous perturbations across the whole section of the underflow. These three types of disturbances are selected to satisfy multiple forcing conditions spanning from quasi-two-dimensional forcing of the boundary layer to homogeneous three-dimensional, small-scale forcing of the underflow with the grid set-up. Our aim is to generalize the forced symmetry features in the wake, independently of the disturbance applied to the shear flow.

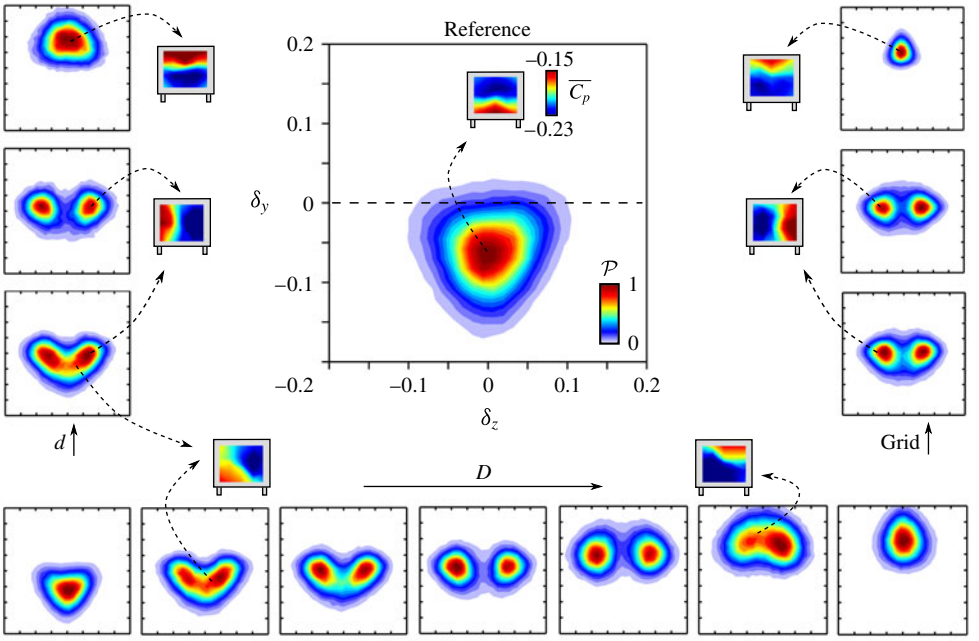

FIGURE 2. Diagram of normalized probability distribution $\mathcal{P}(\delta_y, \delta_z)$ for perturbed wakes. The reference flow is presented at the centre of the picture. The arrows indicate increasing size of the perturbations: $d = \{0.020, 0.027, 0.054\}$, $D = \{0.027, 0.067, 0.084, 0.10, 0.17, 0.20, 0.24\}$, coarse, medium and fine grids. Asymmetric flow states become apparent by conditional averaging and are represented using the contour map of the mean pressure coefficient $\overline{C_p}$.

3. Disturbing wake asymmetries

In figure 2, we present the joint probability distribution $\mathcal{P}(\delta_y, \delta_z)$ of the pressure gradients resulting from all three types of disturbances. Independently of the disturbance geometry, the increase in its size causes an inversion of the wall-normal pressure gradient δ_y: the wake statistically transitions from a wall-normal mean asymmetric state with $\delta_y < 0$ to a spanwise switching dynamics presenting $\delta_y \sim 0$, finally recovering an asymmetric mean flow state where $\delta_y > 0$. These features are further characterized by conditional averaging of flow states using the mean pressure coefficient $\overline{C_p}$, which clearly indicates the asymmetric pressure distribution over the rear surface.

Statistics of the velocity field shown in figure 3 provide some information on the symmetry properties of the near wake in the symmetry plane ($z = 0$). We select three configurations for comparison: the reference flow, the bimodal wake that appears when $d = 0.027$ and the inverted asymmetric state resulting from the application of the passive cylinder with diameter $d = 0.054$.

The time-averaged wall-normal velocity $\overline{v}$, the in-plane streamlines and the cross-stream velocity fluctuations $\overline{v'v'}$ highlight the symmetry changes in the disturbed wakes. In the reference case, the near-wake presents a large clockwise recirculation, which shrinks to a nearly symmetric flow when the boundary layer is disturbed with $d = 0.027$. Using a stronger perturbation ($d = 0.054$), the flow recovers wall-normal

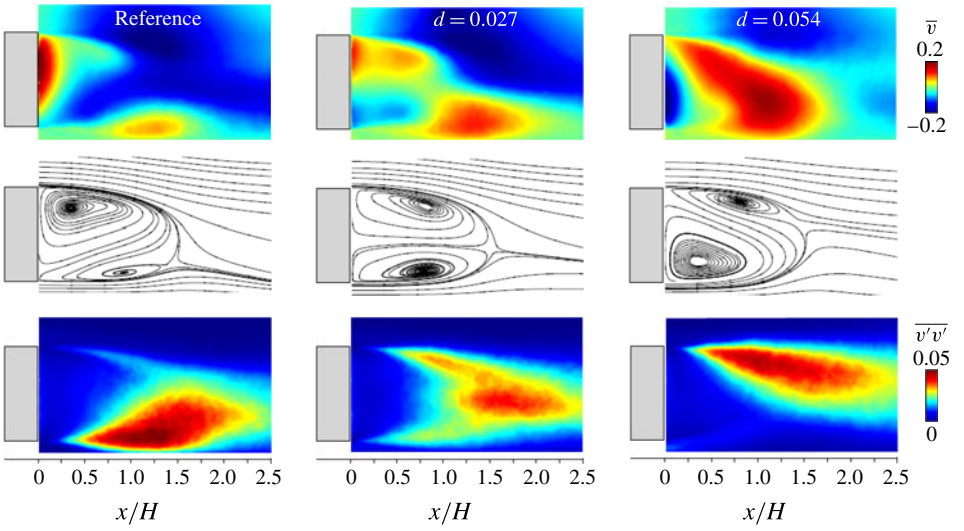

FIGURE 3. Statistics of the velocity field in the symmetry plane ($z = 0$). In these side views, flow comes from left to right. From top to bottom: time-averaged wall-normal velocity $\overline{v}$, in-plane velocity streamlines and wall-normal velocity fluctuations $\overline{v'v'}$. From left to right: reference flow and disturbed wakes with $d = 0.027$ and $d = 0.054$.

asymmetry, but the large recirculating flow structure is now located closer to the wall. These configurations are very similar to the wake topologies reported by other authors and discussed in our introductory paragraphs, but are observed here for the same upstream conditions and set-up, differing only by the presence of passive perturbations.

The observed changes in the wake symmetry in a central vertical plane are accompanied by an inverse modification in the horizontal plane. Figure 4 shows the corresponding evolution of the velocity field at $y/H = 0.67$. Statistical symmetry occurs in the reference flow as well as in the disturbed wake with cylinder diameter $d = 0.054$, while the flow is asymmetric for $d = 0.027$. This asymmetry corresponds to one state of the bimodal dynamics where the conditional average of δ_z is negative.

Our measurements point to the existence of four equivalent asymmetric states in the rectangular bluff-body wake, each of them preserving planar symmetry. It is important to remark in the diagrams of figure 2 that intermediate flow dynamics occur between these states. They are characterized by the meandering of the wake between wall-normal asymmetric states and spanwise (lateral) bimodal configurations exemplified by the cases with $d = 0.020$, $D = 0.067$ or $D = 0.20$. This transition is discussed in the following section on the basis of a symmetry-breaking stochastic model.

4. Description of symmetry-breaking by a stochastic model

It is widely known that stochastic models can predict the statistics of several bimodal flow configurations such as wind reversals in thermal convection and slow dynamics found in von Kármán swirling flows (Sreenivasan, Bershadskii & Niemela 2002; de la Torre & Burguete 2007). Motivated by the recent application of these models to turbulent wakes (Rigas *et al.* 2015; Brackston *et al.* 2016), we consider the one-dimensional Langevin equation to describe the dynamics of the lateral pressure

difference (Gardiner 1985):

$$\dot{\delta_z} = \mathcal{F}(\delta_z) + \sigma\xi(t), \tag{4.1}$$

where $\mathcal{F}(\delta_z)$ is the drift term, σ is the noise intensity and $\xi(t)$ represents the random dynamics of a standard Wiener process. The stationary solution of the Fokker–Planck equation gives the probability distribution function of δ_z,

$$\mathcal{P}(\delta_z) = \frac{1}{C}\exp\left(\frac{-2\mathcal{V}(\delta_z)}{\sigma^2}\right), \quad \mathcal{V}(\delta_z) = \frac{1}{4}\beta{\delta_z}^4 - \frac{1}{2}\alpha{\delta_z}^2. \tag{4.2a,b}$$

In this equation, C is a normalization factor and $\mathcal{V}(\delta_z)$ is the potential function associated with the drift term by $\mathcal{F}(\delta_z) = -\partial\mathcal{V}(\delta_z)/\partial\delta_z = -\beta{\delta_z}^3 + \alpha\delta_z$, in which α and β are coefficients commonly used to model a bimodal distribution or a pitchfork bifurcation.

To clarify the transition scenario of perturbed wakes in our experiments, we use the measured time series of δ_z to compare the dynamical features of models identified from the reference flow, the transitioning configuration and the bimodal wake. The model identification is straightforward: we compute σ from linear fitting of the mean square displacement $\langle[\delta_z(t+\tau) - \delta_z(t)]^2\rangle = \sigma^2\tau$ of the time series; then we obtain the coefficients α, β and C following (4.2) using a least mean squares algorithm (Rigas *et al.* 2015). Finally, we simulate (4.1) using the Euler–Maruyama scheme (Kloeden & Platen 1992)

$$(\delta_z)_{i+1} - (\delta_z)_i = [-\beta{(\delta_z)_i}^3 + \alpha(\delta_z)_i]\Delta t + \sigma\sqrt{\Delta t}\xi_i \tag{4.3}$$

with a time step $\Delta t = 1.6\times10^{-4}$, a normal distributed noise $\xi_i \sim \mathcal{N}(0,1)$, $i \in \{1, 10^7\}$ and $(\delta_z)_i = 0$ for $i = 1$. The convective time ($t^\star = tU_o/H$) evolution of the experimental and the numerical model series is shown in figure 5. The parameters obtained from the model identification are detailed in the caption.

The stochastic model describes well the bifurcation of δ_z from a single-well to a double-well potential depicted in figures 5(*a*,*c*). Both experimental and numerical time series highlight a transition dynamics shown in figure 5(*b*), where δ_z presents irregular motions associated with wake meandering between spanwise asymmetric configurations. This transition is associated with a shallow barrier in the potential, which occurs mathematically due to a sign inversion of the coefficient α in the model and an increase in the magnitude of β. It must be noted, however, that the computed noise intensity remains comparable for all configurations, indicating that the main change in the model comes from the impact of disturbances on the drift term.

The ability of the stochastic model to represent the dynamics of these configurations enables us to include the amount of disturbance to recover the probability diagram of disturbed wakes. Let us consider the scatter plot of figure 6(*a*) obtained from the time series of all disturbances D shown in figure 2. We first consider the probability distribution $\mathcal{P}(\Delta_y, \delta_z)$ in figure 6(*b*) at a fixed Δ_y, which might be interpreted as an imposed wall-normal asymmetry originating from the perturbations.

When the y asymmetry becomes larger than a critical value ϵ, $|\Delta_y| > \epsilon$ prevents spanwise wake meandering. In these cases, such as the reference flow, $d = 0.054$ and $D = 0.24$, the near wake is dominated by a strong asymmetric wall-normal recirculation, which forces the potential $\mathcal{V}(\delta_z)$ to present one symmetric mean state (negative α). This is corroborated by the symmetric velocity fields in a wall-parallel plane shown in figure 4. For weaker wall-normal asymmetry ($|\Delta_y| < \epsilon$), spanwise

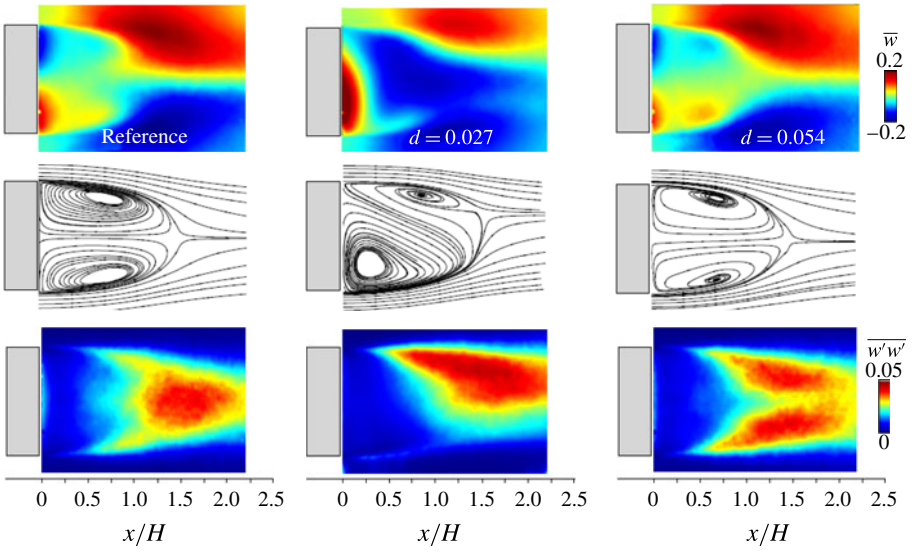

FIGURE 4. Statistics of the velocity field in the middle plane at ($y/H = 0.67$). In these top views, flow comes from left to right. From top to bottom: mean spanwise velocity $\overline{w}$, in-plane velocity streamlines and lateral velocity fluctuations $\overline{w'w'}$ for the reference flow and disturbed wakes with $d = 0.027$ and $d = 0.054$. The compared configurations are the same as in figure 3. The flow presents spanwise asymmetry for $d = 0.027$ because it corresponds to a conditional time average of the states with negative δ_z.

meandering takes place between states given by $\delta_z = \pm(\alpha/\beta)^{0.5}$ with $\alpha > 0$, reaching maximum pressure gradients at $\delta_z = \pm(\alpha^\star/\beta^\star)^{0.5}$. Here, $\alpha^\star$ and $\beta^\star$ are the coefficients of the bimodal configuration with the highest potential barrier, i.e. cases $D = 0.1$ and $d = 0.027$, for which $|\Delta_y| \to 0$. In the intermediate cases, called transition, the wake meanders erratically with a shallow probability distribution well. This behaviour points to a competition between wall-normal and spanwise pressure gradients in the recirculating flow. To account for the effect of $|\Delta_y|$ in our analogy we propose to adjust our coefficients based on ϵ:

$$\alpha = \alpha^\star \left(1 - \frac{\Delta_y^2}{\epsilon^2}\right), \quad \beta = \beta^\star \exp(-\Delta_y^2). \tag{4.4a,b}$$

The quadratic and exponential functions respectively describe the sign change of α for a threshold ϵ and the decay of β with stronger wall-normal asymmetry according to our previous model identification.

We compare in figure 6(*b*,*c*) the experimental and the modelled probabilities $\mathcal{P}(\Delta_y, \delta_z)$ using (4.2) with $\sigma = 0.1$ coupled to (4.4) and threshold $\epsilon = 0.075$ estimated from the experimental data. The analytical model recovers the probability space from the experimental results with all perturbed cases, clearly showing the symmetry-breaking bifurcation for several imposed wall-normal asymmetries Δ_y. The amount of asymmetry along y may therefore fix the degree of symmetry in z.

A more sophisticated stochastic model can be proposed in the present case by coupling the one-dimensional Langevin equation for δ_z obtained previously (4.1)–(4.3) and replacing Δ_y by $\delta_y = \Delta_y + \delta_y'$ in (4.4), i.e. an instantaneous evolution of the

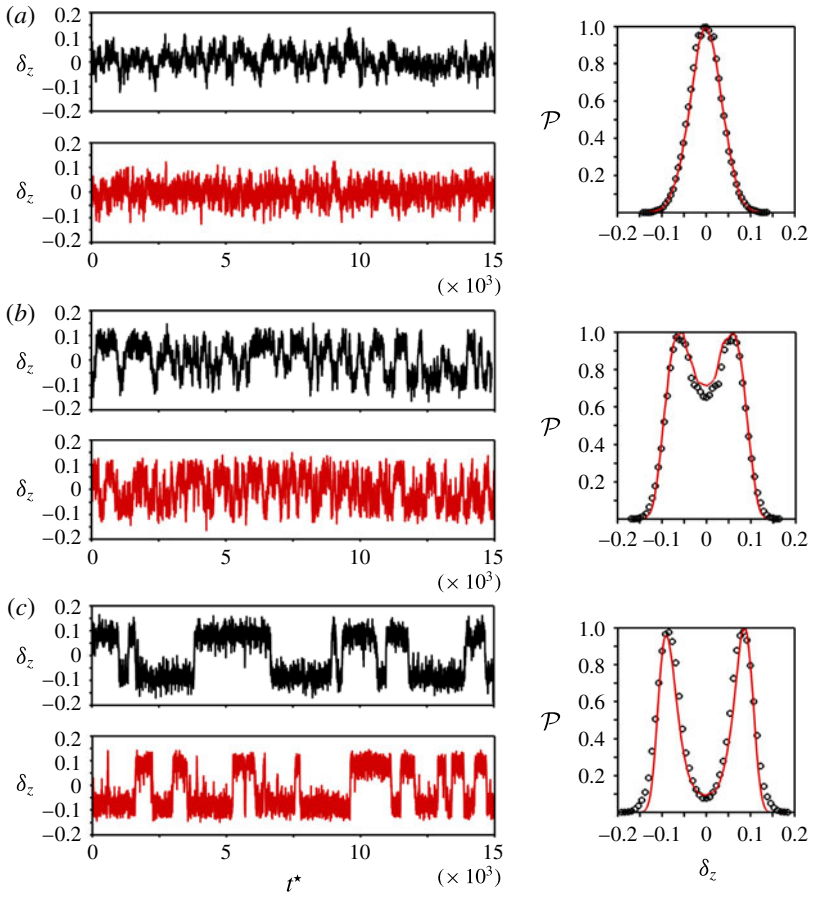

FIGURE 5. Model identification comparing experimental data (black) and simulations (red) for the reference flow, the transient disturbed wake ($D = 0.067$) and the bimodal wake ($D = 0.1$). The model coefficients are (*a*) reference flow: $\sigma = 0.083$, $\alpha = -2.64$ and $\beta = 9.62$; (*b*) $D = 0.067$: $\sigma = 0.096$, $\alpha = 1.71$ and $\beta = 442.86$ and (*c*) $D = 0.1$: $\sigma = 0.10$, $\alpha = 5.87$ and $\beta = 742.34$.

wall-normal pressure gradient. No vertical symmetry-breaking can be observed for the experimental configuration (due to the present values of the aspect ratio and ground clearance) as detailed in Grandemange *et al.* (2013*b*). However, we choose to describe the instantaneous evolution of the wall-normal pressure gradient by a pitchfork amplitude equation for the fluctuating part δ_y'. We write

$$\dot{\delta}_y' = \alpha_o \delta_y' - \beta_o {\delta_y'}^3 + \gamma_o \xi(t), \tag{4.5}$$

in which $\alpha_o = -6.94$, $\beta_o = 118.19$ and $\gamma_o = 0.12$ are the coefficients of the Langevin equation identified from the wall-normal pressure gradient signal of the reference configuration.

The simulation of this new coupled system considering both δ_z and δ_y for multiple imposed asymmetries Δ_y is presented in figure 7. The parameters of the simulation are the same as before: $\sigma = 0.1$, $\epsilon = 0.075$, $\Delta t = 1.6 \times 10^{-4}$, normal distributed

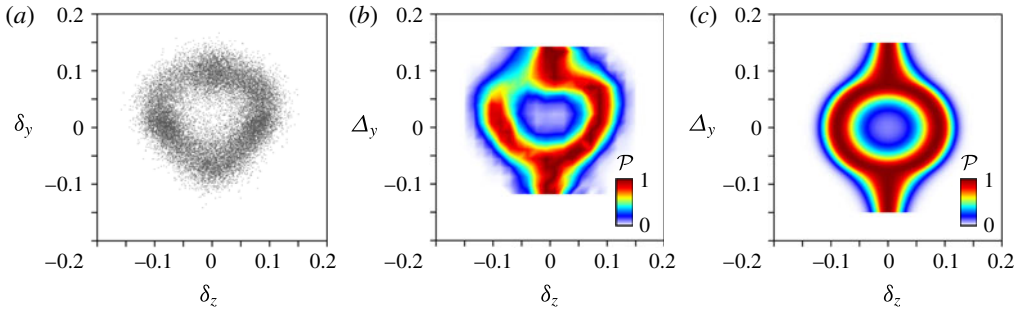

FIGURE 6. (*a*) Scatter plot from experimental time series of disturbed wakes using perturbations *D*. For clarity, the signals are downsampled to 10 Hz. Probability distribution of the lateral pressure difference δ_z for a given wall-normal asymmetry Δ_y for experiments (*b*) and model (*c*).

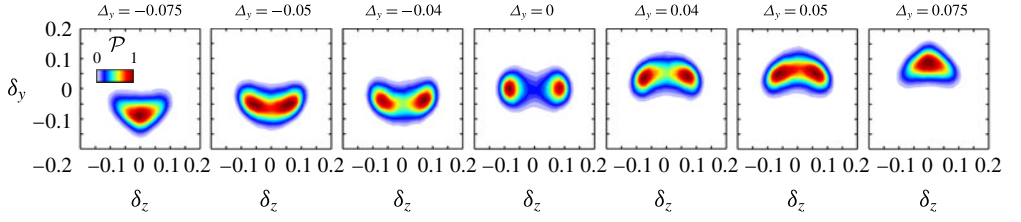

FIGURE 7. Probability space from simulations of the coupled (δ_z, δ_y) model for multiple imposed wall-normal asymmetries Δ_y.

noise $\xi_i \sim \mathcal{N}(0, 1)$ and $i \in \{1, 10^7\}$. The joint probability distribution generated by the coupled stochastic model compares very well with the experimental results for different imposed asymmetries (see figures 2 and 7). The model reproduces the transition from wall-normal to spanwise asymmetric flow states and the intermediate dynamics in this transition characterized by wake meandering between flow states. It demonstrates the capability of our analogy to reproduce an instantaneous evolution of both δ_z and δ_y for different forced configurations observed previously.

A physical scenario can be derived from our symmetry-breaking analogy and near-wake results. As perturbations are installed under the bluff body, the vertical pressure balance δ_y in the wake approaches equilibrium, leading to a nearly symmetric flow in the wall-normal plane with the bimodal behaviour first reported in Grandemange *et al.* (2013*b*). A further increase in disturbance size reverses the recirculating flow structure by increasing the magnitude of δ_y. The comparison to the axisymmetric counterpart is straightforward. Indeed, it was shown by Grandemange *et al.* (2014) that $m = 1$ disturbances applied at θ_W in the sphere wake break the symmetry along the perturbation azimuth but maintain symmetry in its normal plane. Interestingly, $m = 2$ disturbances applied at $\pm\theta_W$ recover symmetry in the disturbed plane, leading to bimodal dynamics in the plane defined by $\pm(\theta_W + 0.5\pi)$ with equivalent features compared to the bimodal behaviour presented here for $\delta_y \sim 0$. The very recent results on misalignment discussed by Gentile *et al.* (2017) exemplify again the sensitivity of the axisymmetric wake to azimuthal disturbances and support our disturbance framework, favourably comparing rectangular and axisymmetric geometries. The competition between normal pressure gradients imposed

by perturbations in the wake appears to be a general feature independently of the bluff-body geometry and allows us to explain the symmetry-breaking bifurcation that occurs when the amplitude of near-wake perturbation is increased.

5. Concluding remarks

Our results underline the high sensitivity of turbulent wakes to disturbances of distinct nature, exemplified here in the flow past a rectangular bluff body in proximity to a wall. The symmetry properties of the near wake are controlled using passive devices and reveal a bifurcation scenario where the flow transitions from a wall-normal asymmetric recirculation to the bimodal, spanwise wake reversals reported recently by Grandemange *et al.* (2013*b*). The flow states identified in this bifurcation scenario help us to unify the distinct topologies observed in the literature of 3D rectangular wake flows so far, presenting key similarities with their axisymmetric counterpart.

The dynamics of this transition can be recovered using stochastic Langevin equations with multiple drift terms, pointing to a competition between wall-normal and spanwise pressure gradients in the near wake. While wall-normal asymmetric wakes induce spanwise statistical symmetry, asymmetric spanwise states associated with bimodal wake switching are observed when the flow is nearly symmetric in the plane normal to the wall. The intermediate dynamics in this transition is characterized by wake meandering between asymmetric wall-normal and spanwise flow states, which does not exhibit a perfect bimodal distribution, similar to the chaotic behaviour investigated recently by Varon *et al.* (2017).

The impact of these perturbations on the near-wake flow additionally provides us with tools to complement current strategies for control of fluid forces exerted on bluff bodies. The amount of asymmetry in the wake with large pressure gradients plays a major role in the base drag and possibly influences the rear lift and side forces over the geometry (Evrard *et al.* 2016; Li *et al.* 2016; Evstafyeva, Morgans & Longa 2017).

Acknowledgements

This work is supported by PSA – Peugeot Citroën and ANRT in the context of the OpenLab Fluidics (fluidics@poitiers). The authors are grateful to R. Li, F. Harambat and J. M. Breux for fruitful discussions and support during the experiments.

References

ACHENBACH, E. 1974 Vortex shedding from spheres. *J. Fluid Mech.* **62** (02), 209–221.

AHMED, S. R., RAMN, G. & FALTIN, G. 1984 Some salient features of the time averaged ground vehicle wake. *SAE Tech. Rep.* No. 840300, Society of Automotive Engineers, Inc., Warrendale, PA.

BARROS, D., BORÉE, J., NOACK, B. R. & SPOHN, A. 2016*a* Resonances in the forced turbulent wake past a 3D blunt body. *Phys. Fluids* **28** (6), 065104.

BARROS, D., BORÉE, J., NOACK, B. R., SPOHN, A. & RUIZ, T. 2016*b* Bluff body drag manipulation using pulsed jets and Coanda effect. *J. Fluid Mech.* **805**, 422–459.

BRACKSTON, R. D., DE LA CRUZ LOPEZ, J. M. G., WYNN, A., RIGAS, G. & MORRISON, J. F. 2016 Stochastic modelling and feedback control of bistability in a turbulent bluff body wake. *J. Fluid Mech.* **802**, 726–749.

CHOI, H., LEE, J. & PARK, H. 2014 Aerodynamics of heavy vehicles. *Annu. Rev. Fluid Mech.* **46**, 441–468.

EVRARD, A., CADOT, O., HERBERT, V., RICOT, D., VIGNERON, R. & DÉLERY, J. 2016 Fluid force and symmetry breaking modes of a 3D bluff body with a base cavity. *J. Fluids Struct.* **61**, 99–114.

EVSTAFYEVA, O., MORGANS, A. S. & DALLA LONGA, L. 2017 Simulation and feedback control of the Ahmed body flow exhibiting symmetry breaking behaviour. *J. Fluid Mech.* **817**, R2.

FABRE, D., AUGUSTE, F. & MAGNAUDET, J. 2008 Bifurcations and symmetry breaking in the wake of axisymmetric bodies. *Phys. Fluids* **20** (5), 051702.

GARDINER, C. W. 1985 *Handbook of Stochastic Methods*. Springer.

GENTILE, V., VAN OUDHEUSDEN, B. W., SCHRIJER, F. F. J. & SCARANO, F. 2017 The effect of angular misalignment on low-frequency axisymmetric wake instability. *J. Fluid Mech.* **813**, R3.

GRANDEMANGE, M., CADOT, O. & GOHLKE, M. 2012 Reflectional symmetry breaking of the separated flow over three-dimensional bluff bodies. *Phys. Rev.* E **86** (3), 035302.

GRANDEMANGE, M., GOHLKE, M. & CADOT, O. 2013*a* Bi-stability in the turbulent wake past parallelepiped bodies with various aspect ratios and wall effects. *Phys. Fluids* **25** (9), 095103.

GRANDEMANGE, M., GOHLKE, M. & CADOT, O. 2013*b* Turbulent wake past a three-dimensional blunt body. Part 1. Global modes and bi-stability. *J. Fluid Mech.* **722**, 51–84.

GRANDEMANGE, M., GOHLKE, M. & CADOT, O. 2014 Statistical axisymmetry of the turbulent sphere wake. *Exp. Fluids* **55** (11), 1–11.

KLOEDEN, P. & PLATEN, E. 1992 *Numerical Solution of Stochastic Differential Equations*. Springer.

KRAJNOVIC, S. & DAVIDSON, L. 2003 Numerical study of the flow around a bus-shaped body. *Trans. ASME J. Fluids Engng* **125** (3), 500–509.

LAHAYE, A., LEROY, A. & KOURTA, A. 2014 Aerodynamic characterisation of a square back bluff body flow. *Int. J. Aerod.* **4** (1–2), 43–60.

LI, R., BARROS, D., BORÉE, J., CADOT, O., NOACK, B. R. & CORDIER, L. 2016 Feedback control of bimodal wake dynamics. *Exp. Fluids* **57** (10), 158.

MARQUET, O. & LARSSON, M. 2015 Global wake instabilities of low aspect-ratio flat-plates. *Eur. J. Mech. (B/Fluids)* **49**, 400–412.

MCARTHUR, D., BURTON, D., THOMPSON, M. & SHERIDAN, J. 2016 On the near wake of a simplified heavy vehicle. *J. Fluids Struct.* **66**, 293–314.

PERRY, A. K., PAVIA, G. & PASSMORE, M. 2016 Influence of short rear end tapers on the wake of a simplified square-back vehicle: wake topology and rear drag. *Exp. Fluids* **57** (11), 169.

RIGAS, G., MORGANS, A. S., BRACKSTON, R. D. & MORRISON, J. F. 2015 Diffusive dynamics and stochastic models of turbulent axisymmetric wakes. *J. Fluid Mech.* **778**, R2.

RIGAS, G., OXLADE, A. R., MORGANS, A. S. & MORRISON, J. F. 2014 Low-dimensional dynamics of a turbulent axisymmetric wake. *J. Fluid Mech.* **755**, R5.

SREENIVASAN, K. R., BERSHADSKII, A. & NIEMELA, J. J. 2002 Mean wind and its reversal in thermal convection. *Phys. Rev.* E **65** (5), 056306.

DE LA TORRE, A. & BURGUETE, J. 2007 Slow dynamics in a turbulent von Kármán swirling flow. *Phys. Rev. Lett.* **99** (5), 054101.

VARON, E., EULALIE, Y., EDWIGE, S., GILOTTE, P. & AIDER, J. L. 2017 Chaotic dynamics of large-scale structures in a turbulent wake. *Phys. Rev. Fluids* **2** (3), 034604.

VOLPE, R., DEVINANT, P. & KOURTA, A. 2015 Experimental characterization of the unsteady natural wake of the full-scale square back Ahmed body: flow bi-stability and spectral analysis. *Exp. Fluids* **56** (5), 1–22.

WASSEN, E., EICHINGER, S. & THIELE, F. 2010 Simulation of active drag reduction for a square-back vehicle. In *Active Flow Control II*, pp. 241–255. Springer.